nature genetics

Mutations in the PCNA-binding domain of *CDKN1C* cause IMAGe syndrome

Valerie A Arboleda[1], Hane Lee[1,2], Rahul Parnaik[3], Alice Fleming[1], Abhik Banerjee[1], Bruno Ferraz-de-Souza[3,4], Emmanuèle C Délot[5], Imilce A Rodriguez-Fernandez[1], Debora Braslavsky[6], Ignacio Bergadá[6], Esteban C Dell'Angelica[1], Stanley F Nelson[1,2], Julian A Martinez-Agosto[1,5], John C Achermann[3] & Eric Vilain[1,5,7]

IMAGe syndrome (intrauterine growth restriction, metaphyseal dysplasia, adrenal hypoplasia congenita and genital anomalies) is an undergrowth developmental disorder with life-threatening consequences[1]. An identity-by-descent analysis in a family with IMAGe syndrome[2] identified a 17.2-Mb locus on chromosome 11p15 that segregated in the affected family members. Targeted exon array capture of the disease locus, followed by high-throughput genomic sequencing and validation by dideoxy sequencing, identified missense mutations in the imprinted gene *CDKN1C* (also known as *P57KIP2*) in two familial and four unrelated patients. A familial analysis showed an imprinted mode of inheritance in which only maternal transmission of the mutation resulted in IMAGe syndrome. *CDKN1C* inhibits cell-cycle progression[3], and we found that targeted expression of IMAGe-associated *CDKN1C* mutations in *Drosophila* caused severe eye growth defects compared to wild-type *CDKN1C*, suggesting a gain-of-function mechanism. All IMAGe-associated mutations clustered in the PCNA-binding domain of *CDKN1C* and resulted in loss of PCNA binding, distinguishing them from the mutations of *CDKN1C* that cause Beckwith-Wiedemann syndrome, an overgrowth syndrome[4].

Since the initial description of IMAGe syndrome (MIM300290)[1], a number of isolated and familial cases have been reported[1,5–11]. To identify a causative gene for IMAGe syndrome, we performed a 250K *Nsp* Affymetrix SNP Array on seven affected and one unaffected sibling from family A, a five-generation family from Argentina (**Fig. 1a**). Further analysis using a custom script detected a 17.2-Mb identical-by-descent (IBD) region on chromosome 11 that was shared by seven affected family members but not an unaffected sibling (**Fig. 1b**), with an LOD (logarithm (base 10) of odds) score of 5.4. Despite the multisystem involvement of IMAGe syndrome, we did not identify a contiguous gene deletion or duplication in the affected individuals (**Supplementary Fig. 1**).

To determine the causative mutation in IMAGe syndrome, we performed targeted high-throughput genomic sequencing of all the exons within a conservative IBD region. We designed an Agilent 244K custom CGH array to capture all exons and splice sites within the region spanning 0–22.6 Mb on chromosome 11. In total, we prepared, pooled and captured five custom barcoded genomic DNA libraries (V-1 and V-6 from family A and unrelated patients 1, 2 and 3) on a single custom array and sequenced the DNA enriched for the IBD region on one lane of the Illumina Genome Analyzer II. Our targeted approach yielded an average coverage of 32×. Patient 3 had a substantially lower coverage of 9× across the targeted intervals, and we did not use this individual in the initial bioinformatics analysis. In the remaining four samples analyzed, ~85% of all targeted regions were covered at ≥10×.

The pedigree and IBD analysis led us to hypothesize that IMAGe syndrome was inherited as a rare autosomal-dominant disorder. Our bioinformatics analysis required that both individuals V-1 and V-6 share the same rare gene variant and at least one of the unrelated IMAGe syndrome patients harbor a rare variant (defined as a variant not present in dbSNP129) in the same gene. This approach identified a single gene, *CDKN1C*.

On further examination, we noted that *CDKN1C* was captured and sequenced at a much lower rate compared to other targeted genes as a result of its high GC content of ≥80%. To compound this low gene coverage, we resequenced *CDKN1C* by dideoxy sequencing (the primers used are listed in **Supplementary Table 1**) in all five individuals previously sequenced by high-throughput sequencing and in an additional individual with sporadic disease (patient 4). The affected individuals from family A carried a c.825T>G mutation resulting in a p.Phe276Val missense alteration. The four unrelated patients with IMAGe syndrome harbored one of the following alterations in *CDKN1C*: p.Phe276Ser, p.Arg279Pro, p.Asp274Asn and p.Lys278Glu (**Table 1**). In total, we identified five rare heterozygous missense mutations in *CDKN1C* that cluster within six amino acids of the

[1]Department of Human Genetics, David Geffen School of Medicine, University of California, Los Angeles, California, USA. [2]Department of Pathology and Laboratory Medicine, David Geffen School of Medicine, University of California, Los Angeles, California, USA. [3]Developmental Endocrinology Research Group, Clinical and Molecular Genetics Unit, University College London Institute of Child Health, London, UK. [4]Department of Endocrinology, Laboratory of Medical Investigation (LIM18), University of São Paulo School of Medicine, São Paulo, Brazil. [5]Department of Pediatrics, David Geffen School of Medicine, University of California, Los Angeles, California, USA. [6]Division of Endocrinology, Hospital de Niños Ricardo Gutierrez, Buenos Aires, Argentina. [7]Department of Urology, David Geffen School of Medicine, University of California, Los Angeles, California, USA. Correspondence should be addressed to E.V. (evilain@ucla.edu).

Received 9 November 2011; accepted 17 April 2012; published online 27 May 2012; doi:10.1038/ng.2275

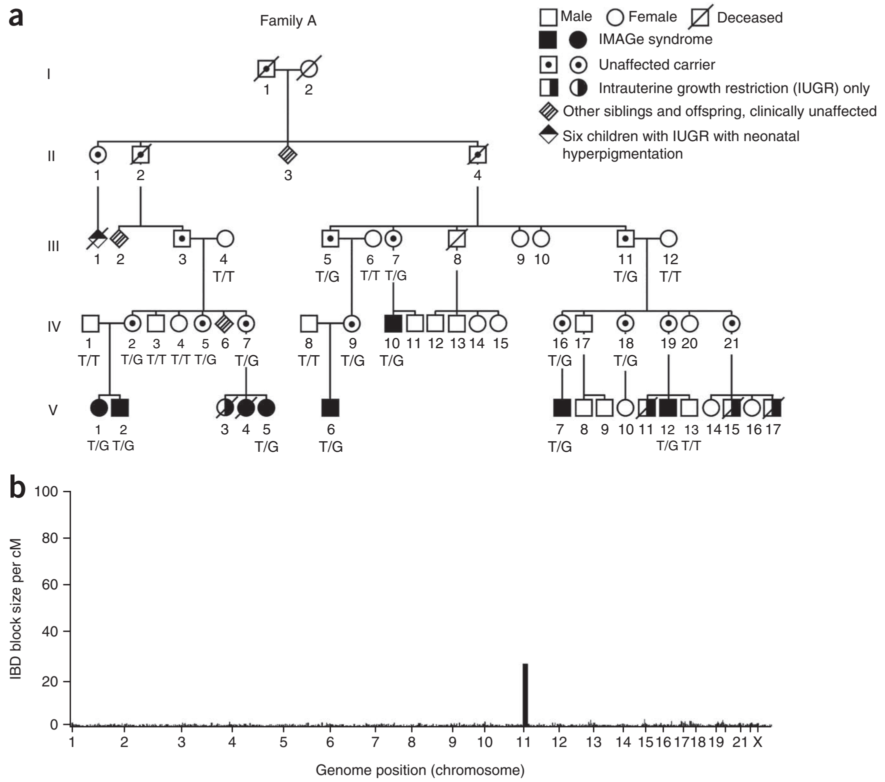

Figure 1 IBD analysis in a family with IMAGe syndrome. (**a**) In this large family (family A) with IMAGe syndrome[2], 24 individuals were tested for genetic mutations in *CDKN1C*. All affected individuals we tested carried the c.825T>G mutation on the maternally inherited allele resulting in a p.Phe276Val amino acid change. Unaffected carriers all inherited the mutations on the paternal alleles. (**b**) The IBD analysis identified a region on chromosome 11 spanning 2,685,916–19,809,755 bp (according to hg19) that was shared by the affected family members (IV-10, V-1, V-2, V-5, V-6, V-7 and V-12) but not by an unaffected sibling (V-13).

PCNA-binding domain[12] (**Fig. 2a**). All variants localized to a highly conserved region[13] (**Fig. 2b**) and are predicted to be damaging to the structure and function of *CDKN1C* by PolyPhen analysis[14].

CDKN1C is located on chromosome 11 and encodes a protein known to have a key role in inhibiting cell-cycle progression. In most tissues, the paternal allele is repressed by distant imprinting control regions, such that expression of *CDKN1C* is primarily from the maternal allele[15,16]. Inheritance of IMAGe syndrome in family A was only through maternal transmission of the *CDKN1C* mutation (**Fig. 1a**). Sequencing for the c.825T>G mutation in 24 members from family A confirmed that only individuals who inherited the mutation on the maternal allele were affected. A c.825T>G mutation inherited on the paternal allele was not expressed, presumably because of epigenetic silencing of the mutated allele.

To confirm the pathogenicity of these mutations, we used an *in vivo* functional model in which IMAGe-associated human *CDKN1C* mutants were expressed in *Drosophila melanogaster* using the GAL4–upstream activation sequence (UAS) system[17]. Ubiquitous overexpression of wild-type or mutant *CDKN1C* resulted in early larval lethality. Targeted expression of the IMAGe-associated *CDKN1C* mutants resulted in altered wing vein patterning and smaller wing size (**Supplementary Figs. 2** and **3**). Expression of wild-type *CDKN1C* restricted to the eye did not have any effects on adult eye size, whereas expression of the IMAGe-associated *CDKN1C* mutants resulted in a moderate to severe reduction in eye size (**Fig. 3**).

Overexpression of IMAGe-associated *CDKN1C* mutants in HEK293T cells did not interfere with the ability of CDKN1C to inhibit the cell cycle in phase G0/G1 through binding of the CDK domain (**Supplementary Fig. 4**). These data suggest that IMAGe-associated mutations within the PCNA-binding domain do not inhibit cell-cycle progression and probably act through a different mechanism that results in IMAGe syndrome.

CDKN1C is located within an imprinted cluster of genes that regulate prenatal and postnatal growth and development. Genetic alterations in *CDKN1C* have been shown to give rise to

Table 1 Clinical characteristics of individuals with IMAGe syndrome

	Patient 1	Patient 2	Patient 3	Patient 4	IV-10	V-12	V-7	V-6	V-5	V-1	V-2
Chromosomal sex	46, XY	46, XY	46, XY	46, XY	46, XY	46, XY	46, XY	46, XY	46, XX	46, XX	46, XY
Nucleotide change	c.826T>C	c.835G>C	c.819G>A	c.831A>G	c.825T>G	c.825T>G	c.825T>G	c.825T>G	c.825T>G	c.825T>G	c.825T>G
Amino acid change	p.Phe276Ser	p.Arg279Pro	p.Asp274Asn	p.Lys278Glu	p.Phe276Val	p.Phe276Val	p.Phe276Val	p.Phe276Val	p.Phe276Val	p.Phe276Val	p.Phe276Val
Intrauterine growth restriction	+	+	+	+	+	+	+	+	+	+	+
Adrenal crisis[a]	+ (day 14)	+ (day 4)	+ (day 7)	+ (day 3)	+ (day 11)	+ (first week)	+ (day 11)	+ (day 19)	+ (day 20)	+ (day 5)	+ (day 21)
Adrenal hypoplasia	Probable	+	+	+	+	+	+	+	+	+	+
Hypercalciuria	+	+	Probable	+	NE	NE	NE	NE	-	NE	NE
Bifrontal bossing, abnormal ears and nose	+	+	+	+	+	+	+	+	+	+	+
Short arms and legs	+	+	+	+	–	–	–	–	+	–	–
Craniosynostosis	+	+	+	–	–	–	–	–	–	–	–
Genital anomalies	+	+	Small penis	+	+	+	+	–	NA	NA	–
Cryptorchidism, unilateral or bilateral	+	+	+	+	+	–	–	+	NA	NA	+
Osteopenia	+	+	+	NE	NE	NE	NE	NE	NE	NE	N/E
Delayed bone age	+	+	+	+	+	+	+	+	+	–	+
Small epiphyses	+	–	+	+	+	+	–	+	NE	–	+
Striated irregular metaphyses	+	+	+	+	+	+	–	+	NE	–	+

[a]The time in parentheses refers to the postnatal day of adrenal crisis.NE, not evaluated; NA, not applicable.

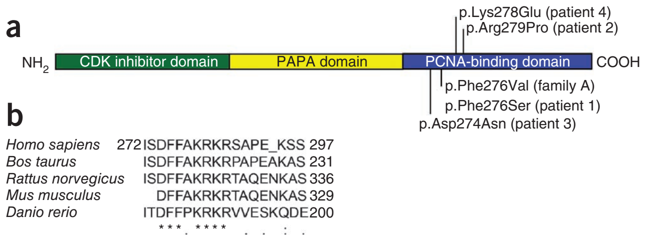

Figure 2 Localization of IMAGe syndrome–associated mutations in *CDKN1C*. (**a**) All IMAGe syndrome–associated mutations are localized to the region of the gene encoding the PCNA-binding domain. (**b**) Highly conserved amino acid residues (indicated by an asterisk) in the PCNA-binding domain of *CDKN1C* are conserved down to *Danio rerio*. All IMAGe-associated mutations affect highly conserved residues. A colon indicates conservation between groups of strongly similar properties, and a period indicates conservation between groups of weakly similar properties.

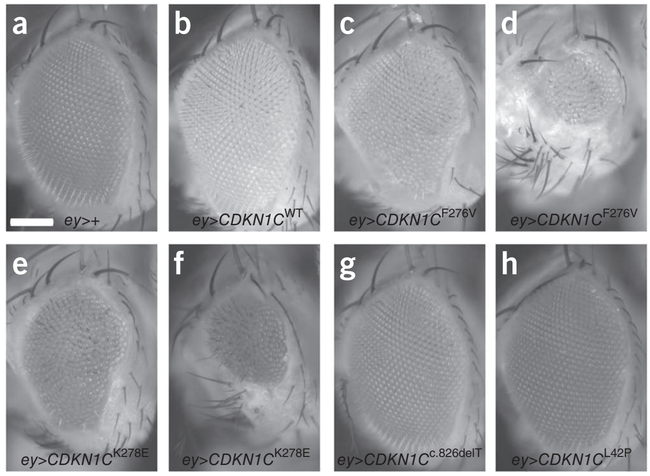

Figure 3 Phenotypic validation of IMAGe syndrome–associated mutations in *D. melanogaster*. (**a**) Light microscope image of an adult wild-type eye (*ey>+*). Scale bar, 25 μm. (**b**) Eye-specific expression of human *CDKN1C* (*ey>CDKN1C*^{WT}) did not affect final eye size. (**c**–**f**) Overexpression of the IMAGe syndrome–associated human *CDKN1C* alterations p.Phe276Val (**c**,**d**, *ey>CDKN1C*^{F276V}) or p.Lys278Glu (**e**,**f**, *ey>CDKN1C*^{K278E}) in the developing eye led to a gain-of-function phenotype of moderate (**c**,**e**) to severely (**d**,**f**) restricted eye growth. (**g**,**h**) Overexpression of the human *CDKN1C* BWS-associated mutation c.826delT (**g**, *ey>CDKN1C*$^{c.826delT}$) or alteration p.Leu42Pro (**h**, *ey>CDKN1C*^{L42P}) did not affect eye growth.

Beckwith-Wiedemann syndrome (BWS; MIM#130650), an overgrowth disorder[18,19]. Here we show that an undergrowth condition, IMAGe syndrome, is caused by domain-specific mutations in the maternally inherited allele of *CDKN1C*.

Both human patients with BWS and *Cdkn1c*$^{-/-}$knockout mice have adrenal hyperplasia[20,21], which is in contrast to the adrenal hypoplasia in patients with IMAGe syndrome. We therefore verified that *CDKN1C* mRNA and protein are expressed in the developing human adrenal gland (**Fig. 4**). Quantitative RT-PCR showed that the expression of *CDKN1C* is greater in adrenal tissue than in brain or muscle during early human development (**Fig. 4a**). Immunohistochemistry showed the strongest expression of *CDKN1C* within a subset of cells in the subcapsular or developing definitive zone of the adrenal gland (**Fig. 4b**).

To determine whether BWS- and IMAGe-associated mutations work through the same mechanism, we repeated the above functional studies with BWS-specific mutants. In the cell-cycle analysis, transfection of the BWS CDKN1C mutant p.Leu42Pro resulted in a loss of cell-cycle inhibition at phase G0/G1. Ubiquitous expression of BWS-associated *CDKN1C* mutations in *D. melanogaster* were early larval lethal, however, targeted expression of the mutations had no effect on eye size, wing size or wing vein patterning (**Fig. 3g**,**h** and **Supplementary Figs. 2e**, **2f**, **3e** and **3f**). Thus, *in vitro* and *in vivo*, BWS mutants have different effects relative to IMAGe mutants, suggesting that domain-specific mutations have differential effects on cell-cycle progression and developmental processes.

BWS-associated mutations in *CDKN1C* are either missense mutations that are localized to the cyclin-dependent kinase binding

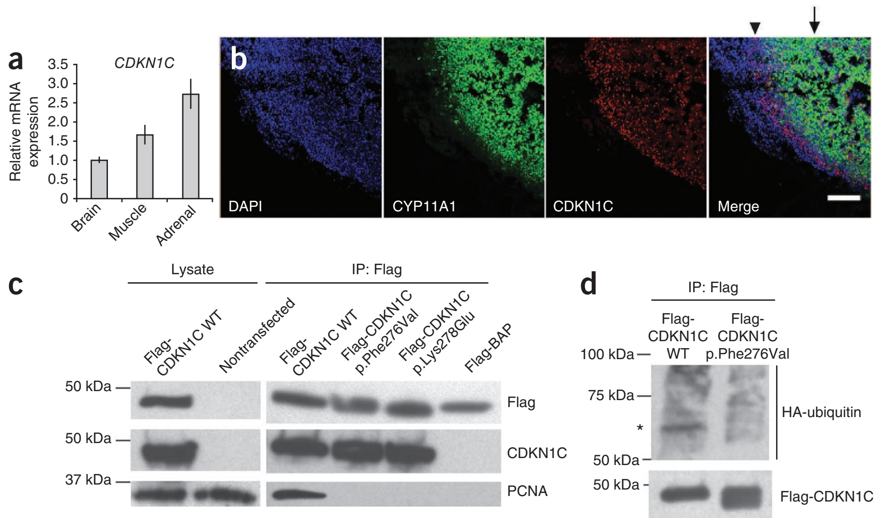

Figure 4 *CDKN1C* is expressed in the developing human adrenal gland, and IMAGe mutants lose PCNA binding, altering the ubiquitination of CDKN1C. (**a**) TaqMan RT-PCR showed higher expression of *CDKN1C* in the adrenal gland at 7–8 weeks after conception compared to control samples (muscle and brain). Error bars, s.d. (**b**) Immunohistochemistry showed CDKN1C protein expression in the developing adrenal gland at 8 weeks after conception. Nuclear expression of CDKN1C was observed in a subset of cells in the subcapsular region and developing definitive cortex (arrowhead). Expression of the steroidogenic enzyme CYP11A1 is shown, predominantly in the fetal zone of the developing gland (arrow). Nuclear counterstaining was performed with 4′,6-diamidino-2-phenylindole (DAPI). Scale bar, 200 μm. (**c**) HEK293T cells transfected with Flag-tagged wild-type CDKN1C (Flag-CDKN1C WT) or IMAGe mutant CDKN1C (Flag-CDKN1C p.Phe276Val or Flag-CDKN1C p.Lys278Glu) were immunoprecipitated with Flag antibody. Whole lysates for wild-type and nontransfected cells (left). The Flag immunoprecipitated fraction binds with endogenous PCNA in wild-type CDKN1C but not in the IMAGe CDKN1C mutants p.Phe276Val and p.Lys278Glu (right). Flag-BAP, Flag-tagged bacterial alkaline phosphatase. (**d**) Immunoprecipitation of HEK293T cells cotransfected with Flag-CDKN1C (wild-type or p.Phe276Val) and HA-ubiquitin constructs. Immunoblot with HA antibody identifies a band at ~63 kDa (indicated by an asterisk) in the wild-type CDKN1C that is not present in the p.Phe276Val IMAGe mutant (top). Immunoblot of Flag protein (bottom).

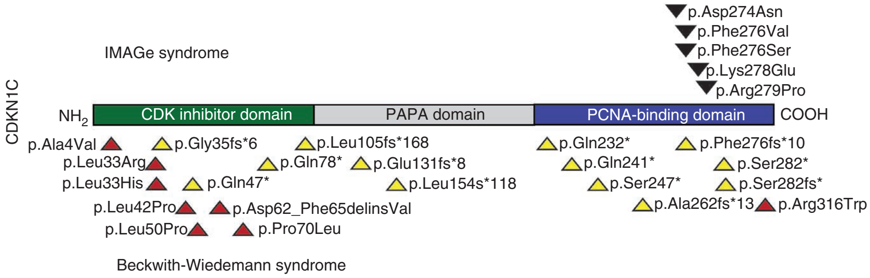

Figure 5 Missense mutations in the CDK-binding domain and truncating mutations in CDKN1C cause BWS, whereas missense mutations localized to the PCNA-binding domain result in IMAGe syndrome. Comparison between *CDKN1C* mutations resulting in IMAGe syndrome (black arrowheads located above the gene) and those resulting in BWS[4] (below the gene, with red arrowheads indicating missense mutations and yellow arrowheads indicating truncating mutations). BWS-associated mutations are either missense mutations primarily located in the cyclin-binding domain or truncating mutations, whereas IMAGe syndrome–associated mutations are all missense mutations that are localized to a highly conserved region of the PCNA-binding domain.

domain or nonsense mutations, both of which result in protein loss of function, overproliferation and predisposition to cancer[22] as a result of a loss of cell-cycle inhibition[3]. In contrast, we show that missense mutations that are localized to a highly conserved region of the PCNA-binding domain of *CDKN1C* in IMAGe syndrome result in excess inhibition of growth and differentiation—a gain of function (**Fig. 5**).

As two of the five mutations fall into a putative nuclear localization signal, we determined whether IMAGe mutants interfere with active nuclear transport of CDKN1C. Human H295R cells and M1 fibroblasts transfected with GFP-CDKN1C fusion constructs (**Supplementary Fig. 5**) showed that none of the tested IMAGe mutants interfered with active transport mechanisms or with binding affinity to α-importin.

Because IMAGe mutations cluster in a domain known to bind PCNA, we performed coimmunoprecipitation experiments to test the effects of IMAGe mutations on PCNA binding. We transfected HEK293T cells with Flag-tagged CDKN1C constructs bearing the wild-type or IMAGe-associated mutant alleles (p.Phe276Val and p.Lys278Glu). Endogenous PCNA was recovered from the wild-type but not the IMAGe mutant immunoprecipitates (**Fig. 4c**), suggesting that PCNA binding is disrupted in the mutants.

As one of the roles of *PCNA* is to facilitate the ubiquitination of cell-cycle proteins[23], we investigated the role of IMAGe mutations in the PCNA-dependent ubiquitination of CDKN1C. We cotransfected HEK293T cells with Flag-tagged wild-type or IMAGe-associated mutant p.Phe276Val CDKN1C and with hemagglutinin (HA)-tagged ubiquitin (12 kDa) and subjected them to coimmunoprecipitation. CDKN1C migrates at ~50 kDa, and, therefore, we expected monoubiquitinated, diubiquitinated and polyubiquitinated CDKN1C to migrate at ~62 kDa or higher, depending on the number and branching of the ubiquitin moieties. Here we show that a band at 63 kDa, the approximate size of a monoubiquitinated CDKN1C protein, is present in immunoprecipitates from wild-type CDKN1C but is absent in those from the IMAGe mutant sample (**Fig. 4d**).

Our data reveal a role for PCNA binding in a specific ubiquitination modification of *CDKN1C*. Many cell-cycle proteins are subject to PCNA-dependent ubiquitination[24], which has pleiotropic effects. Monoubiquitination, as observed in our data, may have a number of functional consequences, such as the modulation of protein localization, protein interactions and proteosomal degradation[25–27]. The latter is less probable because it typically requires, at minimum, tetraubiquitination[28], but it cannot be ruled out without further information on CDKN1C protein stability.

Next-generation sequencing has emerged as a powerful tool in identifying rare Mendelian disease genes by using existing linkage analysis data to identify a disease gene in an unbiased way. Our findings show that missense mutations in the PCNA-binding domain have an inhibitory effect on growth through loss of binding of PCNA to CDKN1C, thereby altering the ubiquitination of CDKN1C and presumably promoting its function. The contrast between BWS- and IMAGe-associated mutations in *CDKN1C* highlights the dual and opposing effects of specific *CDKN1C* mutations. Mutations within the PCNA-binding site of *CDKN1C* blocked *in vivo* growth and differentiation and may illuminate previously unidentified mechanisms regulating cell transformation[12], tumor growth and cell-cycle progression.

URLs. Novoalign, http://www.novocraft.com/index.php; BFAST, http://bfast.sourceforge.net; Picard, http://picard.sourceforge.net/; SAMtools, http://samtools.sourceforge.net/; UCSC Genome Browser, http://genome.ucsc.edu/; SeqWare, http://seqware.sourceforge.net.

METHODS

Methods and any associated references are available in the online version of the paper.

Note: Supplementary information is available in the online version of the paper.

ACKNOWLEDGMENTS

This work was funded by the Doris Duke Charitable Foundation and National Institute of Child Health and Human Development RO1HD068138. V.A.A. was supported by the US National Institutes of Health (NIH) 1 F31HD068136 training grant. The human embryonic and fetal material was provided by the Joint Medical Research Council (grant G0700089) and Wellcome Trust (grant GR082557) Human Developmental Biology Resource (www.hdbr.org). J.C.A. was supported by a Wellcome Trust Senior Research Fellowship in Clinical Science (079666). We thank R. Matera (NIH) for kindly providing the pCI-neo-$(HA)_3$-human ubiquitin construct. We thank E.R.B. McCabe for initial crucial support of the adrenal research for E.V. and for providing one of the original IMAGe patient's DNA samples. We thank M. Le Merrer and C. Lecointre, who participated in the initial clinical description of IMAGe.

AUTHOR CONTRIBUTIONS

V.A.A. designed and performed the experiments, analyzed data and wrote the paper. E.V. designed the project, supervised the overall experiments and wrote the paper with V.A.A. H.L. and S.F.N. contributed to design and analysis of the linkage and sequencing data. E.C. Délot contributed to the design of cell-cycle analysis experiments and editing of the manuscript. A.F., E.C. Dell'Angelica and I.A.R.-F. contributed to the nuclear localization experiments and design of the PCNA and ubiquitin assays. D.B. and I.B. clinically assessed and extracted DNA from family A. R.P., B.F.-d.-S. and J.C.A. performed immunofluorescence and RT-PCR experiments. A.B. and J.A.M.-A. performed, analyzed and contributed to the reporting of the *Drosophila* experiments. All authors discussed the results and implications of the work and commented on the manuscript at various stages.

COMPETING FINANCIAL INTERESTS

The authors declare no competing financial interests.

Published online at http://www.nature.com/doifinder/10.1038/ng.2275.
Reprints and permissions information is available online at http://www.nature.com/reprints/index.html.

1. Vilain, E. *et al.* IMAGe, a new clinical association of intrauterine growth retardation, metaphyseal dysplasia, adrenal hypoplasia congenita, and genital anomalies. *J. Clin. Endocrinol. Metab.* **84**, 4335–4340 (1999).
2. Bergadá, I. *et al.* Familial occurrence of the IMAGe association: additional clinical variants and a proposed mode of inheritance. *J. Clin. Endocrinol. Metab.* **90**, 3186–3190 (2005).
3. Lee, M.H., Reynisdottir, I. & Massagué, J. Cloning of p57KIP2, a cyclin-dependent kinase inhibitor with unique domain structure and tissue distribution. *Genes Dev.* **9**, 639–649 (1995).
4. Romanelli, V. *et al.* *CDKN1C* (p57Kip2) analysis in Beckwith-Wiedemann syndrome (BWS) patients: genotype-phenotype correlations, novel mutations, and polymorphisms. *Am. J. Med. Genet. A.* **152A**, 1390–1397 (2010).
5. Hutz, J.E. *et al.* IMAGe association and congenital adrenal hypoplasia: no disease-causing mutations found in the *ACD* gene. *Mol. Genet. Metab.* **88**, 66–70 (2006).
6. Ko, J.M., Lee, J.H., Kim, G.H., Kim, A.R. & Yoo, H.W. A case of a Korean newborn with IMAGe association presenting with hyperpigmented skin at birth. *Eur. J. Pediatr.* **166**, 879–880 (2007).
7. Lienhardt, A., Mas, J.C., Kalifa, G., Chaussain, J.L. & Tauber, M. IMAGe association: additional clinical features and evidence for recessive autosomal inheritance. *Horm. Res.* **57** (suppl. 2), 71–78 (2002).
8. Pedreira, C.C., Savarirayan, R. & Zacharin, M.R. IMAGe syndrome: a complex disorder affecting growth, adrenal and gonadal function, and skeletal development. *J. Pediatr.* **144**, 274–277 (2004).
9. Tan, T.Y. *et al.* Two sisters with IMAGe syndrome: cytomegalic adrenal histopathology, support for autosomal recessive inheritance and literature review. *Am. J. Med. Genet. A.* **140**, 1778–1784 (2006).
10. Amano, N. *et al.* Radiological evolution in IMAGe association: a case report. *Am. J. Med. Genet. A.* **146A**, 2130–2133 (2008).
11. Balasubramanian, M., Sprigg, A. & Johnson, D.S. IMAGe syndrome: case report with a previously unreported feature and review of published literature. *Am. J. Med. Genet. A.* **152A**, 3138–3142 (2010).
12. Watanabe, H. *et al.* Suppression of cell transformation by the cyclin-dependent kinase inhibitor p57KIP2 requires binding to proliferating cell nuclear antigen. *Proc. Natl. Acad. Sci. USA* **95**, 1392–1397 (1998).
13. Goujon, M. *et al.* A new bioinformatics analysis tools framework at EMBL-EBI. *Nucleic Acids Res.* **38**, W695–W699 (2010).
14. Adzhubei, I.A. *et al.* A method and server for predicting damaging missense mutations. *Nat. Methods* **7**, 248–249 (2010).
15. Diaz-Meyer, N. *et al.* Silencing of *CDKN1C* (p57KIP2) is associated with hypomethylation at KvDMR1 in Beckwith-Wiedemann syndrome. *J. Med. Genet.* **40**, 797–801 (2003).
16. Shin, J.Y., Fitzpatrick, G.V. & Higgins, M.J. Two distinct mechanisms of silencing by the KvDMR1 imprinting control region. *EMBO J.* **27**, 168–178 (2008).
17. Brand, A.H. & Perrimon, N. Targeted gene expression as a means of altering cell fates and generating dominant phenotypes. *Development* **118**, 401–415 (1993).
18. Wiedemann, H.R. The EMG-syndrome: exomphalos, macroglossia, gigantism and disturbed carbohydrate metabolism. *Z. Kinderheilkd.* **106**, 171–185 (1969).
19. Beckwith, J.B. Macroglossia, omphalocele, adrenal cytomegaly, gigantism, and hyperplastic visceromegaly. *Birth Defects Orig. Art. Ser.* **2**, 188–196 (1969).
20. Zhang, P. *et al.* Altered cell differentiation and proliferation in mice lacking p57KIP2 indicates a role in Beckwith-Wiedemann syndrome. *Nature* **387**, 151–158 (1997).
21. Hatada, I. *et al.* An imprinted gene $p57^{KIP2}$ is mutated in Beckwith-Wiedemann syndrome. *Nat. Genet.* **14**, 171–173 (1996).
22. Bourcigaux, N. *et al.* High expression of cyclin E and G1 CDK and loss of function of p57KIP2 are involved in proliferation of malignant sporadic adrenocortical tumors. *J. Clin. Endocrinol. Metab.* **85**, 322–330 (2000).
23. Havens, C.G. & Walter, J.C. Mechanism of CRL4Cdt2, a PCNA-dependent E3 ubiquitin ligase. *Genes Dev.* **25**, 1568–1582 (2011).
24. Kirchmaier, A.L. Ub-family modifications at the replication fork: regulating PCNA-interacting components. *FEBS Lett.* **585**, 2920–2928 (2011).
25. Ye, Y. & Rape, M. Building ubiquitin chains: E2 enzymes at work. *Nat. Rev. Mol. Cell Biol.* **10**, 755–764 (2009).
26. Mukhopadhyay, D. & Riezman, H. Proteasome-independent functions of ubiquitin in endocytosis and signaling. *Science* **315**, 201–205 (2007).
27. Li, W. & Ye, Y. Polyubiquitin chains: functions, structures, and mechanisms. *Cell. Mol. Life Sci.* **65**, 2397–2406 (2008).
28. Thrower, J.S., Hoffman, L., Rechsteiner, M. & Pickart, C.M. Recognition of the polyubiquitin proteolytic signal. *EMBO J.* **19**, 94–102 (2000).

ONLINE METHODS

Study subjects. All participants were patients diagnosed clinically with IMAGe syndrome. This study was approved by the Institutional Review Board at the University of California Los Angeles, the Hospital de Niños Ricardo Gutierrez in Argentina or the Institute of Child Health at University College London. All participants provided informed consent. The phenotypes of the subjects are summarized in **Table 1**.

IBD analysis. Genomic DNA from seven affected individuals (IV-10, V-1, V-2, V-5, V6, V-7 and V-12) and one unaffected individual (V-13) from a large Argentine family (family A) were genotyped on the Affymetrix 250K *Nsp1* SNP arrays, as per the manufacturer's protocol. Familial relationships were confirmed by checking the sharing statistics in all pairs of samples, and an ancestral IBD analysis was performed using a custom script (B. Merriman, available on request). The IBD analysis script was designed to search for long continuous intervals that were compatible with a common extended haplotype among all the affected individuals but not among the unaffected individuals[29]. A conservative error rate of 1% was used to allow the algorithm to tolerate possible genotyping errors. A rare-dominant model of inheritance was assumed, with the rare haplotype frequency of 0.1% and a penetrance of 100% under the assumption that the carriers (parents of the affected individuals) were not showing the phenotype for a reason other than low penetrance of the disease phenotype (for example, imprinting).

Capture and sequencing of genomic DNA. For the capture of the genes within the IBD interval, we used an Agilent Custom 244K Comparative Genomic Hybridization Array. The 60-bp oligonucleotide probes were tiled every 20 bp against all exonic regions on chromosome 11 between 2.45 and 20.15 Mb (hg18, March 2006, build 36.1) and every 30 bp in the flanking 5′ and 3′ regions spanning 0–2.45 Mb and 20.15–22.6 Mb, respectively. We included all gene models identified in RefSeq, GenBank, CCDS and UniProt. The locations and sequences of all probes used are available on request.

Genomic DNA libraries were created for patients V-1 and V-6 from family A and for three isolated cases with IMAGe[1] (patients 1, 2 and 3) following the manufacturer's protocol (Illumina Protocol for Preparing Samples for Sequencing Genomic DNA, p/n 11251892 Rev. A), except for the adaptor ligation step, where we used custom-made, internally validated barcoded adaptors. After the PCR amplification, five barcoded libraries were pooled together and captured by hybridization to a custom-designed CGH array, as previously described[30]. After the capture, the array was washed, and the captured DNA was eluted, amplified and diluted to a final concentration of 10 nM based on the Qubit concentration measure and Agilent Bioanalyzer. One flowcell lane of single-end sequencing was performed at the University of California Los Angeles Genomic Sequencing Center on the Illumina Genome Analyzer II for 76 cycles, following the manufacturer's protocol. The base calling was performed by the Real Time Analysis software (Illumina).

Sequence data analysis. The Illumina output files (.qseq) were converted to fastq formats using BFAST[31,32] script ill2fastq.pl and then parsed into multiple fastq files, each for one unique barcode. Only the reads with 100% matching barcode sequences were carried over to the second set of fastq files. The sequence reads in each fastq file were aligned to the human reference genome (hg18, March 2006, build 36.1) using Novoalign from the Novocraft Short Read Alignment Package. The output format was set to SAM, and default settings were used for all options. Using SAMtools, the SAM file of each sample was converted to a BAM file, sorted and merged, and potential PCR duplicates were removed using Picard[33]. The variants, both single nucleotide variants (SNVs) and small indels (insertions and deletions), within the captured coding exonic intervals were called using the SAMtools pileup tool. For SNV calling, the last five bases were trimmed, and only the reads lacking indels were retained. For indel calling, only the reads that contained one contiguous indel not occurring on either end of the read were retained[34]. The variants were further annotated using the SeqWare project and loaded into the SeqWare Query Engine database[35]. Variants from each sample with the following criteria were identified: (i) variant base or indel observed at least twice and at ≥5% of the total coverage per base, (ii) variant observed at least once on both the forward and reverse strands and (iii) SNV quality score ≥10. As IMAGe syndrome is a rare condition, only variants with coding consequences not present in dbSNP129 were further analyzed.

***CDKN1C* sequencing.** All *CDKN1C* (RefSeq NM_000076.2) mutations were PCR amplified using Phusion HF polymerase (NEB) with 5% dimethyl sulfoxide (DMSO) and 0.1 M betaine. PCR products were sent for dideoxy sequencing at Laragen. The PCR primers used are listed in **Supplementary Table 1**. All mutation locations were reported using CCDS7738.1 and P49918 as the normal transcript and protein sequences, respectively.

Plasmid constructs. The complementary DNA (cDNA) of CDKN1C cloned into pBluescript was purchased from American Type Culture Collection (99411)[36]. Mutations were generated using site-directed mutagenesis (Stratagene; the primers used are listed in **Supplementary Table 1**). Four mutants were created, corresponding to a BWS-associated alteration and mutation (p.Leu42Pro and c.826delT) and IMAGe syndrome–associated alterations (p.Phe276Val and p.Lys278Glu). Wild-type and mutant versions of *CDKN1C* were subcloned into the plasmids pCDNA3.1(+) and pEGFP-C2 for mammalian cell culture experiments, into pFlag-pcDNA3.1 plasmid for the immunoprecipitation and into pUAST plasmid for the generation of transgenic flies.

Quantitative RT-PCR. Human tissue at 7–8 weeks post-conception (wpc) was provided by the Joint Medical Research Council and Wellcome Trust–funded Human Developmental Biology Resource with Research Ethics Committee approval and informed consent. RNA was extracted from adrenal, brain and muscle samples using the TRIzol reagent, and first-strand cDNA was generated using SuperScript II reverse transcriptase (Invitrogen). Expression of the *CDKN1C* transcript was assessed by quantitative RT-PCR using the StepOnePlus Real-time PCR System, TaqMan Gene Expression Assays for human *CDKN1C* (Hs00175938_m1) and human *GAPDH* as the endogenous control (4333764T; all Applied Biosystems). Data were analyzed with StepOne software v2.1 according to the $2^{-\Delta\Delta CT}$ method.

Immunofluorescence. Fourteen-micron sections of human fetal adrenal tissue (8 wpc) were fixed briefly in 4% paraformaldehyde (PFA) and blocked in 1% bovine serum albumin (BSA) before incubating overnight with antibody to CDKN1C (Fisher, AFMA121866, 1:1,000 dilution) and CYP11A1 (Sigma, HPA016436, 1:100 dilution). Primary antibodies were detected using Alexa647 goat anti-mouse (Invitrogen, A21235, 1:400 dilution) and Alexa555 (Invitrogen, A21429, 1:400 dilution) goat anti-rabbit conjugates. Nuclei were counterstained with DAPI. Images were collected on a Zeiss 710 confocal microscope (Carl Zeiss).

Immunoprecipitation. HEK293T cells were transfected with constructs encoding Flag-CDKN1C with Lipofectamine 2000 (Invitrogen). For ubiquitination assays, cells were cotransfected with a pCI-neo-$(HA)_3$-human ubiquitin[37] construct and treated for 3 h in 10 μM MG132 (Millipore) before cell lysis. Flag-CDKN1C was immunoprecipitated from cell lysates using the Anti-Flag M2-Agarose Affinity Gel (Sigma-Aldrich). Western blot was performed on immunoprecipitated samples and cell lysates using primary antibody to HA (Covance, MMS101R, 1:1,000 dilution), Flag (Abcam, ab1162, 1:10,000 dilution), PCNA (Abcam, ab29, 1:5,000 dilution) and CDKN1C (Santa Cruz Biotechnology, sc-1040, 1:1,000 dilution). The secondary antibodies used were goat anti-mouse HRP (Bio-Rad, 170-5047, 1:20,000) and goat anti-rabbit HRP (Santa Cruz, sc-2030, 1:5,000).

***Drosophila* experiments.** Five independent constructs, wild-type CDKN1C, p.Leu42Pro CDKN1C, c.826delT CKDN1C, p. Phe276Val CDKN1C and p.Lys278Glu CDKN1C, were injected into embryos, and each construct generated multiple independent transgenic lines. Overexpression was achieved by using the GAL4-UAS system[17] and the following drivers: *Ubi-gal4* (ubiquitous expression), *ey-gal4* (eye-specific expression), *MS1096-gal4* (wing-specific expression) and *sal^{PE}-gal4* (wing-pouch–specific expression). *MS1096-gal4* is expressed in the entire wing imaginal disc, but has high expression in the dorsal compartment. This higher expression in the dorsal compartment causes enhanced phenotypic effects in the dorsal compared to the ventral side of

doi:10.1038/ng.2275

the wing. *sal*^{PE}*-gal4* is specifically expressed in the pouch of the wing disc, which only gives rise to the wing proper. All UAS-*CDKN1C* constructs were larval lethal when expressed with *Ubi-gal4*, confirming their expression efficiency. At least two independent lines were used for each experiment, and all yielded similar results. All eye images were taken on a Leica Z16 AP0 Camera. Wing images were taken on Leica DFC 300 FX R2 Camera.

Flow cytometry. Wild-type or mutant versions of *CDKN1C* were cotransfected with pCMV-GFP into serum-starved HEK293T cells using Lipofectamine 2000 (Invitrogen). After 24 h, cells were grown in media containing 5% serum for 48 h. Cells were resuspended in a hypotonic buffer with propidium iodide, and GFP^{+} events were analyzed on a Becton Dickinson FACScan Analytic Flow Cytometer. All experiments were performed in two biological replicates. Statistical significance was assessed using a two-proportion z test. Flow cytometry was performed in the University of California Los Angeles Johansson Comprehensive Cancer Center (JCCC) and Center for AIDS Research Flow Cytometry Core Facility.

Analysis of the nuclear to cytoplasmic distribution of GFP fusion proteins. H295R cells were transfected using Lipofectamine 2000. After incubation for 24 h, the cells were fixed in 4% PFA, and immunohistochemistry was performed using an antibody to GFP (Invitrogen), a fluorescein isothiocyanate (FITC)-labeled secondary antibody (Jackson Lab) and a mounting medium with DAPI (VectorLabs). Cells were imaged on an Olympus AX70 microscope.

M1 fibroblasts were transfected with 2 μg per well of purified expression plasmid using the X-tremeGENE HP DNA transfection reagent (Roche). Twenty-four hours after transfection, cells were fixed in 2% formaldehyde and analyzed using fluorescence microscopy. Fluorescent and bright-field images of randomly selected fields containing transfected M1 cells were saved electronically using a 'blind-code' file nomenclature. The distribution of GFP fusion proteins in each transfected cell was annotated by an experienced observer (who was unaware of the blind code) as one of the following: 1, nuclear only; 2, nuclear and cytoplasmic; or 3, cytoplasmic only.

29. Lee, H., Jen, J.C., Cha, Y.H., Nelson, S.F. & Baloh, R.W. Phenotypic and genetic analysis of a large family with migraine-associated vertigo. *Headache* **48**, 1460–1467 (2008).
30. Lee, H. *et al.* Improving the efficiency of genomic loci capture using oligonucleotide arrays for high throughput resequencing. *BMC Genomics* **10**, 646 (2009).
31. Homer, N., Merriman, B. & Nelson, S.F. BFAST: an alignment tool for large scale genome resequencing. *PLoS ONE* **4**, e7767 (2009).
32. Homer, N., Merriman, B. & Nelson, S.F. Local alignment of two-base encoded DNA sequence. *BMC Bioinformatics* **10**, 175 (2009).
33. Li, H. *et al.* The Sequence Alignment/Map format and SAMtools. *Bioinformatics* **25**, 2078–2079 (2009).
34. Clark, M.J. *et al.* U87MG decoded: the genomic sequence of a cytogenetically aberrant human cancer cell line. *PLoS Genet.* **6**, e1000832 (2010).
35. O'Connor, B.D., Merriman, B. & Nelson, S.F. SeqWare Query Engine: storing and searching sequence data in the cloud. *BMC Bioinformatics* **11** (suppl. 12), S2 (2010).
36. Matsuoka, S. *et al.* p57KIP2, a structurally distinct member of the p21CIP1 Cdk inhibitor family, is a candidate tumor suppressor gene. *Genes Dev.* **9**, 650–662 (1995).
37. Mattera, R., Tsai, Y.C., Weissman, A.M. & Bonifacino, J.S. The Rab5 guanine nucleotide exchange factor Rabex-5 binds ubiquitin (Ub) and functions as a Ub ligase through an atypical Ub-interacting motif and a zinc finger domain. *J. Biol. Chem.* **281**, 6874–6883 (2006).